processes

MDPI

Article

Performance, Emission and Combustion Characteristics of a VCR Engine Fueled with Sea Mango Biodiesel/Diesel Blends

R. Rohith Renish [1], Amala Justus Selvam [2], Robert Čep [3,*] and Muniyandy Elangovan [4,*]

[1] Department of Mechanical Engineering, Vel Tech Rangarajan Dr. Sagunthala R&D Institute of Science and Technology, Chennai 600062, Tamil Nadu, India; rohith.renish@gmail.com
[2] Department of Automobile Engineering, Vel Tech Rangarajan Dr. Sagunthala R&D Institute of Science and Technology, Chennai 600062, Tamil Nadu, India; amalajustus@gmail.com
[3] Department of Machining, Assembly and Engineering Metrology, Faculty of Mechanical Engineering, VSB-Technical University of Ostrava, 70800 Ostrava, Czech Republic
[4] Department of R&D, Bond Marine Consultancy, London EC1V 2NX, UK
* Correspondence: robert.cep@vsb.cz (R.Č.); muniyandy.e@gmail.com (M.E.)

Abstract: The constant emission of greenhouse gases into the atmosphere, due to the continuous burning of fossil fuels, has been driving researchers to develop an environmentally friendly alternative fuel solution. An experimental investigation was conducted on a laboratory scale, to evaluate the physicochemical qualities, performance, emissions, and combustion characteristics of sea mango oil biodiesel blends and pure diesel fuel on a single-cylinder, variable compression ratio (VCR) engine. Tests were conducted at 1500 rpm, 210 bar, and 23° bTDC, under varying loading circumstances of 0, 3, 6, 9, and 12 kgs, and compression ratios 16:1, 17:1, and 18:1, respectively. The findings revealed that higher compression ratios (CRs) improve the performance, emission, and combustion characteristics of an engine. At CR 18:1, BTHE, SFC, and EGT improved by 8.78%, 11.18%, and 2.52% more than the standard compression ratio (17:1). The CO, HC, and smoke emissions also lowered by 14.65%, 18.56%, and 11.56%, respectively, at CR 18:1. The NO_x emissions increased by 6.77%. The combustion characteristics also improved, with an increase in the CR. The findings of this investigation show that sea mango biodiesel blends can be used as a diesel alternative at CR 18:1, with no engine modifications.

Keywords: compression ratio; sea mango biodiesel; performance; emission; combustion

Citation: Renish, R.R.; Selvam, A.J.; Čep, R.; Elangovan, M. Performance, Emission and Combustion Characteristics of a VCR Engine Fueled with Sea Mango Biodiesel/Diesel Blends. *Processes* **2022**, *10*, 1469. https://doi.org/10.3390/pr10081469

Academic Editor: Cherng-Yuan Lin

Received: 24 June 2022
Accepted: 23 July 2022
Published: 27 July 2022

1. Introduction

In response to the demand for rising global energy and pollution, as well as the dwindling supply of petroleum-based fuels, the fuel industry has been scrambling to come up with more environmentally friendly, renewable alternatives to petroleum-based fuels for internal combustion engines [1–3]. Biofuels, such as ethanol and biodiesel, appear to be a viable and adequate substitute for petroleum diesel, due to their similar combustion properties [4–6]. Biodiesel production grew almost 10 times, from 16 billion liters to 143 billion liters, between 2000 and 2017. Global biodiesel production peaked in the year 2016, producing 32.6 million tons. Furthermore, the global biofuel market is expected to expand at an annual rate of 5.4% from 2017 to 2024, according to the International Energy Agency (IEA) [7]. Biodiesel can be produced from both edible and non-edible feedstocks. Until 2015, over 95% of biodiesel was produced from edible oils, including soybean, rapeseed, sunflower, and palm oil. This may have led to an imbalance between food supply and the biodiesel market, due to the increased demand for biodiesel. In response to this issue, non-edible oils such as jatropha, rubber seed, neem, mahua oil, etc., are now in greater demand, and have emerged as viable and sustainable renewable sources for biodiesel production [8]. In terms of fuel qualities, biodiesel provides several benefits over diesel

fuel. The high cetane number, lower exhaust emissions, better lubricating properties, flash point, and cheap manufacturing cost of biodiesel make it preferable to diesel fuel [9].

Simsek, et al. [10], investigated the results of using biodiesel produced from waste canola, safflower, and vegetable oils obtained by transesterification. The tests showed that, in contrast to diesel fuel, SFC and BTHE improved as the biodiesel percentage in the combination increased to B75 and decreased by 1.95% for B100. The average CO, HC, and smoke levels reduced by 34.28%, 17.49%, and 50.95%, respectively, but NOx levels rose by 80.50%, showing that the combination was more stable than diesel fuel. Performance and emission analysis of rubber seed biodiesel—produced under ideal process conditions of a methanol to oil molar ratio of 12:1, a 4 (weight percent) catalyst concentration, and a 3 h reaction time—were carried out by Bharadwaj, et al. [11]. These blends—B10, B20, and B30—were tested in a diesel engine. As the BMEP rose, there was a gradual improvement in BTHE for all blends, and a slight decrease in SFC. The lowest SFC for the B10 blend was 0.3895 (kg/kWh), which was quite similar to the 0.38 (kg/kWh) result obtained with conventional diesel. The highest BTHE for the B10 mix was 73.26%, as compared to regular diesel, which had a value of 75.8%. While NOx (275 ppm) and CO_2 (1.9%) rose, CO (0.0275%) and HC (36 ppm) dropped. The authors concluded that synthetic biodiesel, produced from rubber seed oil, could be a competitive alternative to conventional diesel. Ahmet, et al. [12], conducted the experiment using mixes of 10–20% poppy oil biodiesel and regular diesel fuel. The ID period was extended by the blends. In comparison to diesel, BTHE decreased by around 5.74% and 13.04%, with addition of 10% and 20% poppy oil biodiesel due to the lower calorific content of the poppy oil biodiesel. NOx increased, with the blends of 10% and 20%, by 2.8% and 5.97%, respectively, according to diesel at full load. Contrarily, the mixes—OP10 and OP20—decreased the CO by 15% and 17.41%, respectively. To evaluate the engine characteristics, Mubarak, et al. [13], combined Salvinia molesta biodiesel with diesel at different proportions. The combustion measures showed a maximum decrease in peak pressure and an HRR of 1.89% and 6.79%, respectively, when comparing B20 to diesel. A minimum SFC of 0.308 kg/kWh and a BTHE of 29.52 % were found with B20 in the performance study. The emissions of CO, CO_2, UBHC, NOx, and smoke were all decreased by utilizing B20, when compared to diesel, by 14%, 3.38%, 20.83%, 12.86%, and 10.99%, respectively.

Ahamed, et al. [14], investigated the effects of CRs 18:1, 20:1, and 22:1 on EGR rates in a diesel engine running with a B20 blend of mango seed methyl ester. BTHE rose by 7.4% at CR 22:1, lowering CO, HC, and smoke emissions. The quantity of NO_x was noted to have increased significantly. At CR 22:1 and 5% EGR, the NO_x emissions decreased up to 40.5%. The performance, emission, and combustion of a VCR engine fueled with 20%, 25%, or 30% Karanja biodiesel–diesel blends at CRs 15:1 to 18:1 was studied by Sivaramakrishnan, et al. [15]. The maximum BTHE was 30.46% with the B25 blend at CR 18:1. The emissions of HC and CO reduced as the blend ratio increased. Higher CRs enhanced the blends' in-cylinder pressure (Cp). The authors concluded 18:1 to be the most effective CR. Compression ratios ranged from 14:1 to 18:1. Suresh, et al. [16], looked at the characteristics of argemone Mexicana methyl ester (AME) and its blends in a VCR engine. AME20 at CR 17:1 had higher BP, BTHE, and SFC than diesel. HC and CO emissions improved with a slight rise in NO_x. In a diesel engine with CRs ranging from 13.5:1 to 16.5:1, Sharma, et al. [17], investigated the characteristics of dual biodiesel blends containing mahua and jatropha in equal proportions with diesel. The blends' BP and ME improved by 0.15–1.58% and 1.07–12.42%, respectively, over diesel at CR 16.5:1. The blends had lower Cp and exhaust gas temperature than mineral diesel. The CO and HC emissions for the blends were reduced by 33–62%. Blend B20 turned out to be the most effective among all the blends. Vasudeva, et al. [18], looked at the influence of CRs varying from 15:1 to 18:1 on a CI engine using 10% to 40% rice bran biodiesel–diesel blends. The increase in the CR reduced SFC to 18.6% and increased BTHE by 14.66%. As the CR increased, the CO and HC emissions decreased by 22.27 and 38.4%, respectively, whereas the CO_2 and NO_x emissions increased by 17.43 and 22.76%. Another result was a 15% increase in Cp. The effect of CRs

16:1, 17:1, and 18:1 on a diesel engine were investigated with a 20% palm oil biodiesel blend by Rosha, et al. [19]. At higher CRs, the ignition delay period dropped while Cp and BTHE increased. The blend had a BTHE of 33.8% at full load, and 18:1 CR. From varying 16:1 to 18:1 CR, the HC, CO, and smoke opacity emissions decreased by 47.8%, 41.0%, and 35.7% correspondingly, while NO_x emissions increased by 41.1%. Bora, et al. [20], tested raw biogas at CRs 18:1, 17.5:1, and 17:1 with injection timing of 23° bTDC. The highest BTHE of 20.27% was at CR 18:1 and full load. The highest liquid fuel replacement (LFR) was 80%, 79 %, and 78.2% at CRs 18:1,17.5:1, and 17:1, respectively. CO and HC emissions decreased with the increase in CR, while NO_x emissions rose by 42.85%. An engine with CRs ranging from 16:1 to 18:1 was tested by Datta, et al. [21], with palm oil biodiesel. Clean palm oil biodiesel had BTHE 7.9% lower than diesel, but rose with the CR. The HRR reduced with biodiesel. However, with neat diesel, the inflammatory delay was longer, and was noted to increase with lower CR. The NOx and CO_2 emissions were reduced with lower CRs, whereas the CO and HC increased. Sharma, et al. [22], investigated the behavior of a CI engine modifying its CR. The study was made by B20 blend obtained by pyrolysis of waste tires at different CRs varying from 16.5:1 to 18.5:1. The CR 18.5:1 resulted in shorter ID, maximum Cp, and a quicker HRR. Increasing the CR also enhanced the BTHE by about 8%. With CR 18.5:1, the blend resulted in 10.5%, 32%, and 17.4% lesser BSCO, BSHC, and smoke opacity, respectively. On waste oil biodiesel blends B10 to B50, El, et al. [23], studied the effect of CRs 14:1, 16:1, and 18:1. Higher CRs enhanced BTHE and SFC. CO and HC emissions decreased by 37.5% and 52%, respectively, whereas NO_x and CO_2 emissions increased by 36.8% and 14.3%. Muralidharan, et al. [24], investigated the influence of CR in a VCR engine using waste sunflower oil biodiesel blends with CRs varying from 18:1 to 22:1. The higher the CR, the better was the combustion efficiency, the longer the ignition delays, and the higher the maximum rate of pressure rise. B40 achieved the highest BTHE. The blends reduced HC and CO emissions while increasing the NO_x levels. Suresh, et al. [25], evaluated the work of numerous authors on biofuels in VCR engines, and concluded that biodiesel/diesel blends might be utilized directly in a VCR engine without any alterations. Numerous studies have demonstrated that at higher CRs, VCR engines provide superior engine performance and lower emissions than diesel engines. However, owing to the high peak temperatures, NO_x emissions increase at higher CRs. The authors concluded that VCR engines have the potential to increase fuel combustion efficiency.

Duan, et al. [26], studied the impact of controlling tactics on the auto-ignition time and combustion phase in the HCCI engine. Each controlling approach was addressed in depth in separate parts. Furthermore, the various regulating techniques and their impacts were highlighted. In general, several regulating techniques were constantly paired with each other in HCCI engines, to manage the auto-ignition time and optimize the combustion phase for running at a broad speed and load range. Finally, the key results of the HCCI engine's regulating tactics on ignition timing and combustion phase were also described. Duan, et al. [27], also developed a 1D simulation model of the hydrogen-enriched natural gas SI engine, and tested it against experimental data. Four EGR systems were assessed for combustion, performance, and emissions, using a validated 1D simulation model of a hydrogen-enriched natural gas SI engine. In HP, LP, or HP–LP systems, raising EGR reduced peak in-cylinder combustion pressure. The HP EGR emitted the least NOx. Combining 10% HP EGR and 5% LP EGR (total 15% EGR) was anticipated to maximize thermal efficiency. Reducing valve overlap for internal EGR improved the combustion pressure and the heat release rate.

Sea mango, which is also known as Cerbera Manghas [28] or Cerbera Odollam [29], is a poisonous tree which belongs to the Apocynaceae family [30]. These evergreen trees, which can reach a height of 6–15 m, have spiral-shaped, dark green leaves, and 5–10 cm long, egg-shaped fruits, and can be found along the coasts of southern India, Malaysia, Vietnam, Sri Lanka, Madagascar, and Myanmar. Because of the high concentration of cerberin heart glycoside in the fruit and leaves of these trees, they are very dangerous. In Kerala, India, sea mango seeds have been used as a suicide poison on several occasions [31].

Unlike many non-edible fruits, sea mango is relatively new and unknown. Even though there have been a few studies on sea mango, most of them have focused only on its toxicity and its biodiesel production [29–38], which prompted the authors to choose sea mango as the feedstock.

According to the literature review, an engine's compression ratio, as well as the biodiesel–diesel mix ratio, have a significant effect on improving the engine's characteristics. Though there have been substantial studies on biodiesels tested at a fixed CR on a diesel engine, only a few were focused on VCR engines. Furthermore, employing sea mango biodiesel–diesel blends, the influence of CRs on different engine parameters has not been investigated. Hence, an attempt was made to operate a VCR engine with blends of sea mango biodiesel (SME10, SME20, SME30, and SME40), at different CRs, to evaluate the engine's efficiency and its hazardous exhaust emissions.

2. Experimental Setup and Methods

2.1. Fuel Preparation

The sea mango methyl ester (SME) was produced at the Indian Biodiesel Corporation (IBDC), Baramati, India, employing the esterification and transesterification techniques for sea mango oil. Table 1 shows the fatty acid profile of sea mango oil. The properties of the fuel samples were tested, and are tabulated in Table 2. Due to the high free fatty acid value of the sea mango oil, a two-step approach—namely esterification and transesterification—was necessary. Transesterification is a chemical process that produces monoesters by integrating alcohol and triglycerides in the presence of a catalyst [39–41]. The fundamental goal of these processes is to reduce the oil's viscosity. The transesterification process can be written as shown in Equation (1),

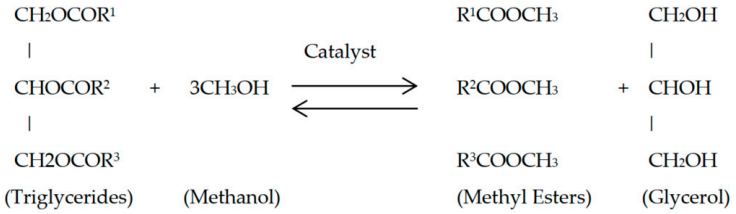

(1)

Table 1. Sea mango oil's fatty acid profile.

Fatty Acid	Formula	Composition (wt.%)
Myristic acid	$C_{14}H_{28}O_2$	0.39
Palmitic acid	$C_{16}H_{32}O_2$	12.98
Stearic acid	$C_{18}H_{36}O_2$	4.23
Oleic acid	$C_{18}H_{34}O_2$	26.15
Linoleic acid	$C_{18}H_{32}O_2$	45.69
Alpha-Linolenic acid	$C_{18}H_{30}O_2$	1.99
Arachidonic acid	$C_{20}H_{32}O_2$	0.490
Cis-8-11-14 Eicosatrienoic	$C_{20}H_{34}O_2$	0.321
Cis-11 Eicosenoic acid	$C_{20}H_{38}O_2$	0.561
Cis-13,16 Docosadienoic acid	$C_{22}H_{40}O_2$	0.121
Behenic acid	$C_{22}H_{44}O_2$	5.998
Tricosanoic acid	$C_{23}H_{46}O_2$	0.860

Table 2. Fuel properties.

Fuel Properties	Unit	DF	SME10	SME20	SME30	SME40	SME100	ASTM
Density at 15 °C	g/cm^3	0.830	0.834	0.839	0.845	0.849	0.875	D1448
Viscosity at 40 °C	mm^2/s	2.7	2.82	2.96	3.07	3.16	4.2	D6751
Calorific Value	MJ/kg	42.5	42.27	42.08	41.79	41.52	38.62	D445
Cetane No.	-	49.22	49.46	49.77	49.94	50.29	51.71	D93
Flash Point	°C	64	74	86	95	103	142	D93
Cloud Point	°C	−4.0	−2.1	1.6	2.9	4.1	7.2	D2500
Fire Point	°C	71	83	92	106	114	156	D613

2.2. Engine Test Rig

The study used a single-cylinder, four-stroke VCR engine developed by Kirloskar. Figure 1 and Table 3 show the photographic perspective of the VCR engine and its specifications, respectively. The engine used an eddy-current-type dynamometer to feed the load at different operating conditions. They were installed on a concrete base with a common bed. An anti-vibration mounting system was employed to isolate the frame structure from the concrete. These engines are engineered in such a way that CR can be modulated even without halting the engine. The cylinder's movement was measured using a micrometer affixed to it. Piezo-type sensors were positioned on the fuel injector and cylinder head, to control the flow of fuel and the combustion pressure. To monitor the exhaust gas temperature, K-type and PT100-type thermocouples were installed within the setup. Rotameters were also installed, to continuously measure the flow of cooling water to the cylinder head, engine block, and calorimeter. Using the data obtained from the multiple points, the IC Engine soft v9.0 program analyzed the test rig's performance, and fed it into the system. The engine exhaust was channeled outside of the test cell, to remove exhaust pollutants from the engine. The engine test rig's schematic architecture is shown in Figure 2. An AVL digas 444N gas analyzer was used to measure the quantity of NO_x, HC, and CO, while an AVL 437 smoke meter was used to assess the level of smoke occurring from the engine. Table 4 lists the instrument range, the uncertainty of the instruments, and their accuracy.

Table 3. Engine Specifications.

Parameter	Specification
General details	4-stroke, multifuel, VCR engine
Number of cylinders	1
Speed	1500 rpm
Ignition	Compression ignition
Compression ratio	12:1–18:1
Rated power	3.5 kW
Loading	Eddy current dynamometer
Bore	87.5 mm
Stroke	110 mm
Rotameter	Calorimeter 25–250 LPH
Temperature sensor	Type K, PT100 thermocouple
2Air flow transmitter	Pressure transmitter
Cooling	Water-cooled

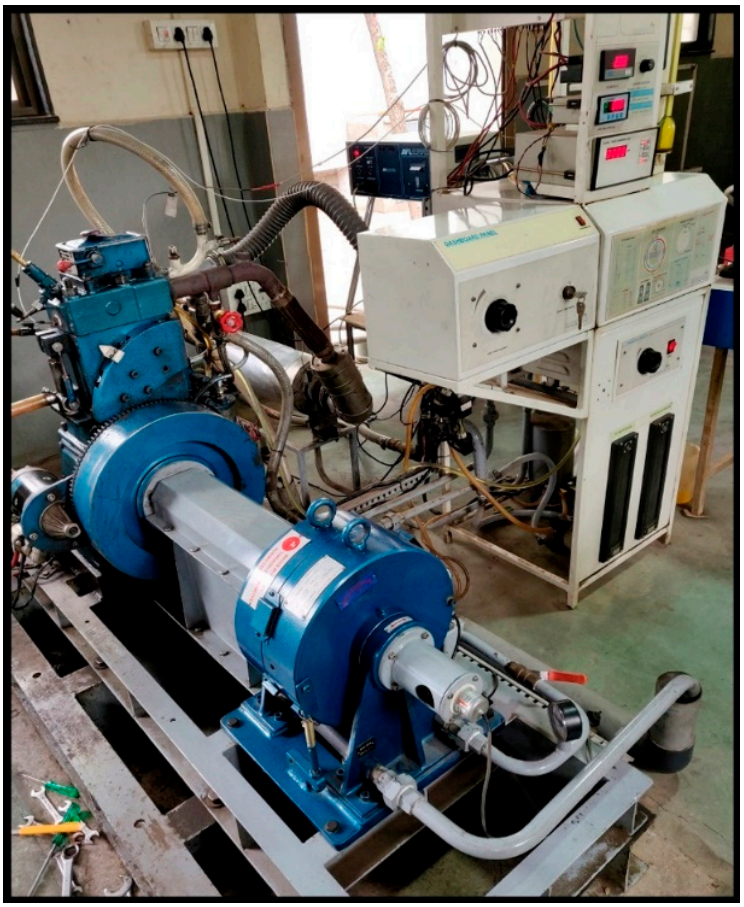

Figure 1. Photographic view of VCR engine.

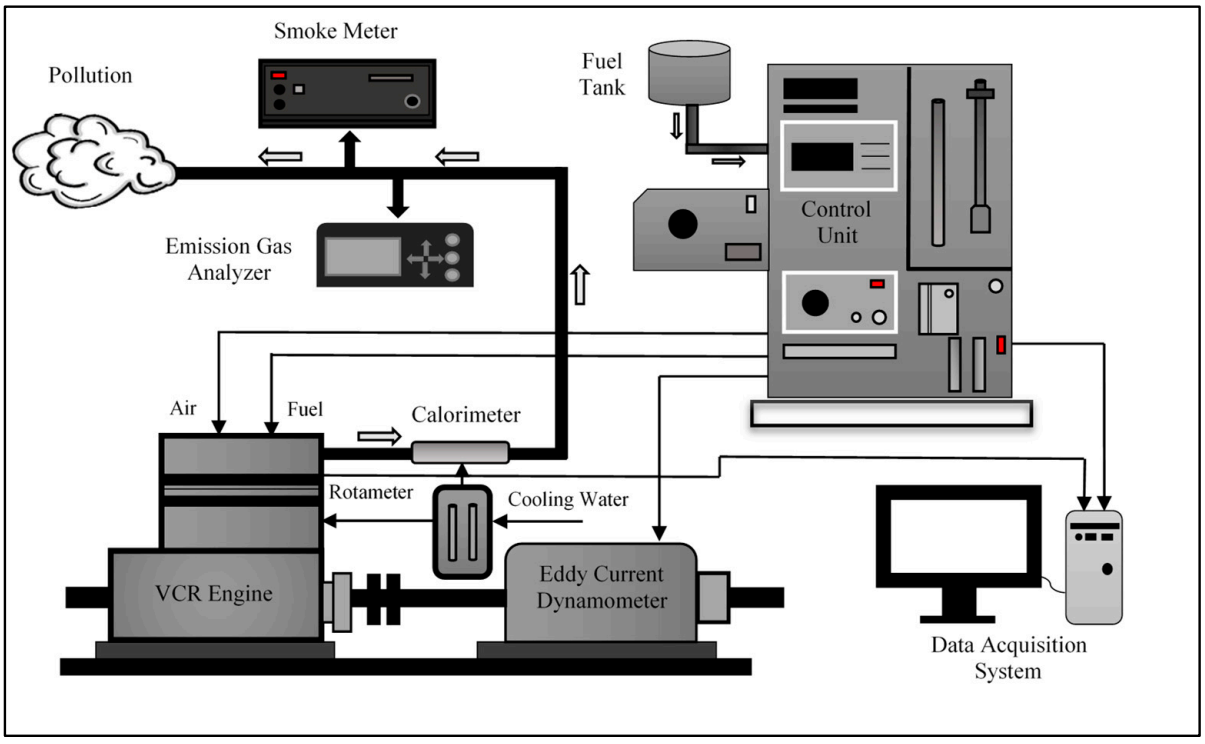

Figure 2. Schematic layout of the engine test rig.

Table 4. Range, accuracy, and uncertainty of the instruments.

Equipment	Measured Quantity	Measuring Range	Accuracy	Uncertainty
AVL digas 444N gas analyzer	CO	0–10%vol	±0.03%vol	±0.15%
	O_2	0–22%vol	±5%vol	±0.5%
	CO_2	0–20%vol	±0.5%vol	±0.3%
	HC	0–20,000 ppm	±5 ppm	±0.4%
	NO_x	0–5000 ppm	±10 ppm	±1.2%
AVL 437 smoke meter	Smoke	0–100%	±2%	±0.8%
Thermocouple	Exhaust gas temperature	0–1200 °C	±2 °C	±0.2%
Tachometer	Engine speed	1–10,000 rpm	±5 rpm	±0.2%
AVL GH14D pressure transducer	Pressure	0–250 bar	±0.3 bar	±0.25%
AVL 365C angle encoder	Crank angle	0–720 °CA	±1 °CA	±0.5%
DP fuel flow transmitter	Fuel flow rate	0–500 mmWC	±2 mmWC	±0.5%

As a precaution, the VCR engine was initially permitted to run with diesel fuel and at full load for the first 20 min, to ensure that the exhaust gas and outlet cooling water temperatures remained consistent, to attain the steady-state condition. This signified that the combustion process within the cylinder had achieved a stable condition, and that the engine was set to collect data. The engine was then gradually restored to a no-load condition, and ran for 5 min. The exhaust gas analyzer and smoke meter were also turned on slightly early, to stabilize the system before commencing the experiment to measure emissions. The analysis started with the recording of the engine's baseline results while fueled with diesel at various loads (0 kg, 3 kg, 6 kg, 9 kg, and 12 kg) at regular intervals i.e., their respective braking powers at CRs 16:1, 17:1, and 18:1. The other parameters, like speed, IT, and IP were kept constant at 1500 rpm, 23° bTDC, and 210 bar, respectively, throughout the trial as they were considered to be the standard for the VCR engine used. Following the diesel tests, sea mango biodiesel blends (SME10, SME20, SME30, and SME40) were tested at CRs 16:1, 17:1, and 18:1, considering 17:1 as the standard CR.

2.3. Uncertainties

Uncertainty analysis is done to predict parameter measurement errors. Every experiment involves some degree of uncertainty. These uncertainties are mostly caused by factors such as environmental conditions, calibration, observations, sensors, and testing procedures. Considering these uncertainties, every experiment's desired test outcome can be predicted. Table 4 displays the relative degree of uncertainty for each measurement. The following formula was used to compute the total uncertainty—Equation (2):

$$\begin{aligned} \mu c &= \sqrt{\sum_{1}^{n} Y^2} \\ &= \sqrt{(\mathrm{BTHE})^2 + (\mathrm{SFC})^2 + (\mathrm{EGT})^2 + (\mathrm{CO})^2 + (\mathrm{HC})^2 + (\mathrm{NOx})^2 + (\mathrm{Smoke})^2 + (\mathrm{CP})^2 + (\mathrm{HRR})^2} \\ &= \sqrt{(0.75)^2 + (0.15)^2 + (0.75)^2 + (0.28)^2 + (0.72)^2 + (1.45)^2 + (0.82)^2 + (0.25)^2 + (0.55)^2} \\ &= \pm 2.21 \end{aligned} \quad (2)$$

where Y was the individual uncertainty for each measured parameter, and μc was the total uncertainty. Table 5 displays the relative degree of uncertainty for each measurement.

Table 5. Variable metrics' uncertainty.

Parameters	Uncertainty %
BTHE	±0.75
SFC	±0.15
EGT	±0.75
CO	±0.28
HC	±0.72
NO_x	±1.45
Smoke	±0.82
Cylinder pressure	±0.25
Heat release rate	±0.55

3. Result and Discussion

In diesel engines, combustion may be affected by a variety of elements, including the quality of fuel, compression ratio, design of the combustion chamber, cetane number, fuel evaporation rate, injection time, and pressure. By optimizing these factors, combustion can be enhanced, and therefore the quantity of fuel used, and the number of exhaust pollutants produced during combustion can be lowered. One of the primary characteristics that affect diesel engines' performance and emissions is the cetane number and combustion efficiency.

3.1. Combustion Analysis

The development of a fuel/air mixture, and the advancement of the combustion phenomenon in the engine cylinder, are the primary factors that influence in-cylinder pressure (Cp) [42]. In addition, the volume of fuel in the pre-mixed combustion phase, regulated by the ignition delay duration and spray envelope of the injected fuel, also influences the in-cylinder pressure. Therefore, the quantity of gasoline stored during the ignite delay interval is also significant. Hence, the longer the ignition delay, the greater the amount of fuel build-up, which ultimately results in lower peak cylinder pressure [43]. Figure 3 demonstrates the variations in the in-cylinder pressure caused at different crank angles for all the fuel samples with differing CRs and full load. The figures show that increasing the proportion of biodiesel in diesel resulted in a drop in in-cylinder pressure. Higher viscosities, lower heating values, and the slower chemical kinetics of blended fuels exacerbated the atomization, and increased the ignition delay, resulting in reduced cylinder pressures for the blended fuels [44]. The higher atomization, evaporation, and energy content of diesel fuel explain why it had the highest cylinder pressure of the tested fuels [45]. The peak cylinder pressure was found to increase with the CR, as seen in Figure 3. This was because more secondary fuel was accessible for burning, when the compression ratio increased. Furthermore, an increase in peak cylinder pressure was seen. This observed phenomenon of peak pressure advancement was predicted, owing to the instantaneous burning of gaseous fuel in the cylinder at greater pressure. The inhalation of more oxygen and a constant fuel flow rate was another probable cause for the increased peak in-cylinder pressure at higher CRs [46]. For the fuels tested at CR 18:1, the peak Cp for diesel, SME10, SME20, SME30, and SME40 was found to be 66.9 bar, 66.68 bar, 66.26 bar, 65.94 bar, and 65.91 bar, respectively.

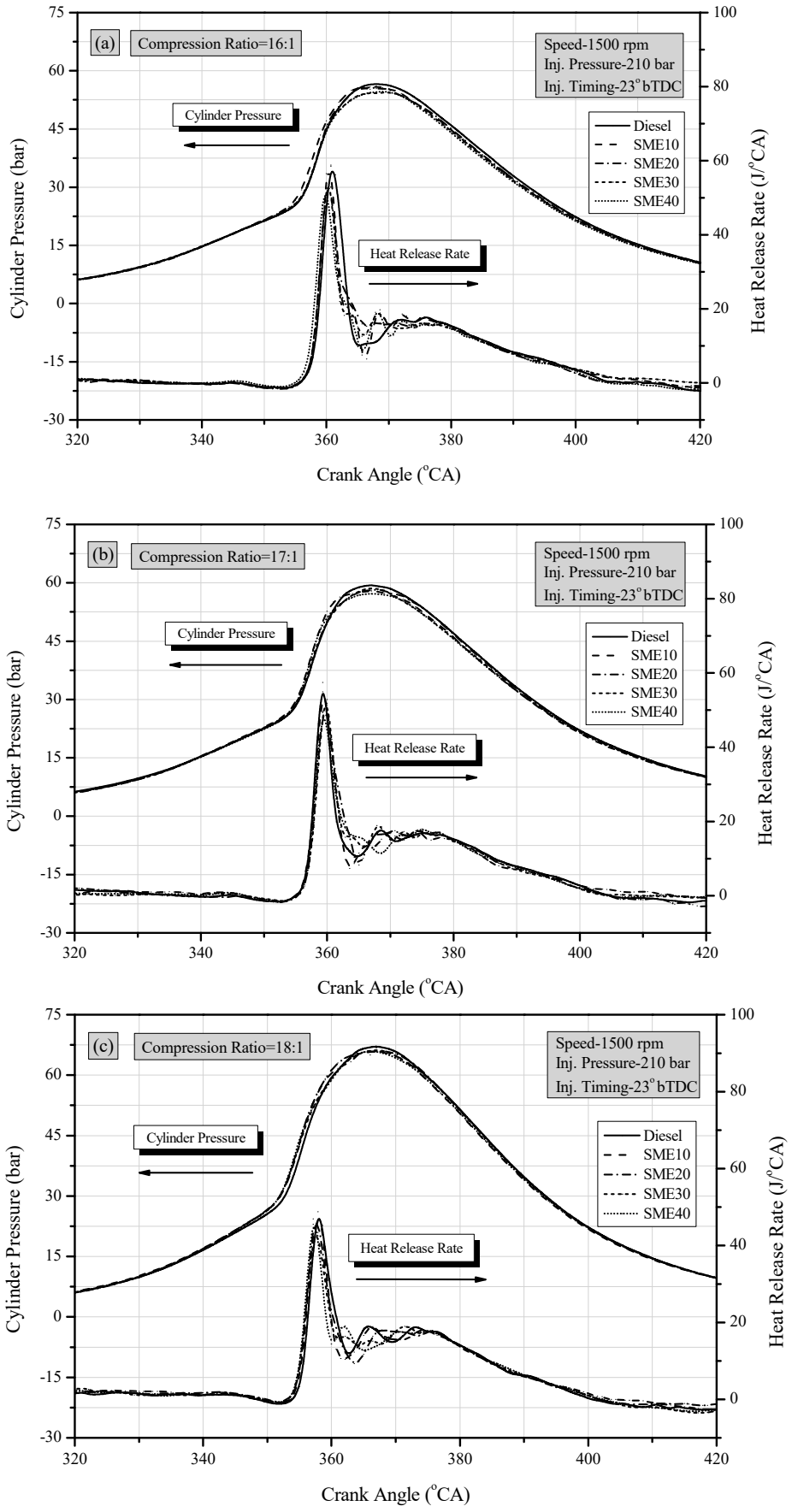

Figure 3. Variation of Cp and HRR with the crank angle for the fuel blends at CRs: (**a**) 16:1 (**b**) 17:1 (**c**) 18:1 and full load.

The heat release rate (HRR) graph illustrates how much heat energy could be transformed into productive work during fuel combustion. It was mostly influenced by the injection timing and ignition delay period [47]. The HRR for different test fuels at each crank angle was computed, using the correlation obtained from the first law of thermodynamics, by Equation (3):

$$\frac{dQ}{d\theta} = P\frac{\gamma}{\gamma-1}\left(\frac{dV}{d\theta}\right) + \frac{1}{\gamma-1}V\frac{dP}{d\theta} \quad (3)$$

where $\frac{dQ}{d\theta}$ represented the HRR (J/deg.), γ represented the specific heat ratio, V was the in-cylinder volume (m^3), P was the in-cylinder gas pressure (bar), and θ was the crank angle (deg.).

Figure 3 also shows the variation in HRR under full load conditions for all the test fuels at different CRs. Initially, the vaporization of the mixture was indicated by a negative heat release rate for all fuel samples. It was followed by a positive heat release rate, as a result of the ignition delay period [48]. The graph shows that the combustion began earlier for the blends, owing to their greater cetane number, shorter delay time, and calorific value, which dramatically lowered the HRR. Due to the existence of the intrinsic availability of O_2 molecules in its structure, and the greater cetane number of biodiesel, the diffusion combustion phase of the blends was noted to be extremely near to that of diesel [49]. As shown in Figure 3, the maximum HRR fell as the engine CR rose. This may have been because the maximum in-cylinder temperature increased as the CR of the engine increased, hence increasing the rate of heat transfer inside the cylinder during combustion [50]. In addition, the reduction in the HRR along with the increase in CRs may also have been attributable to the lower air-fuel mixing, as well as the effect of air entertainment [51]. Diesel, SME10, SME20, SME30, and SME40 had the lowest HRRs of 48.8 J/°CA, 46.9 J/°CA, 46.74 J/°CA, 46.47 J/°CA, and 43.36 J/°CA, respectively, at CR 18:1.

3.2. Performance Analysis

Brake thermal efficiency (BTHE) is defined as the ratio of brake power generated to the quantity of heat provided [52]. In other words, it predicts the efficiency of fuel energy conversion to usable work [53]. Figure 4 illustrates the variance in BTHE with engine load and CRs for all the fuel samples. BTHE increased as the load increased, owing to less energy loss at higher loads [54]. Additionally, it was noted that when the blend ratio increased, BTHE reduced across all load ranges. When biodiesel was added with diesel, the viscosity rose and the volatility reduced, resulting in poor spray characteristics and atomization. Improper spray pattern resulted in non-homogeneous fuel dispersion inside the combustion chamber, perhaps leading to incomplete combustion and decreased BTHE. Furthermore, the reduction in BTHE was attributable to the availability of less fuel power, owing to the low calorific value of sea mango biodiesel [43]. Figure 4 shows that the BTHE rose with the CRs. High combustion chamber temperatures, fine fuel droplets, and increased air–fuel mixing were all factors that contributed to improved BTHE at higher CRs [52]. Diesel, SME10, SME20, SME30, and SME40 had the highest BTHE at CR 18:1, with 30.87%, 30.31%, 29.94%, 29.31%, and 28.61%, respectively.

Specific fuel consumption (SFC) is defined as the amount of fuel required to generate one unit of brake power [53]. It is a crucial metric that indicates how effectively an engine performs. Several influencing characteristics—such as the fuel's cetane number, density, calorific value, and air/fuel ratio—have a significant impact on SFC. For complete combustion, the fuel's heating value is also a key factor. It is also inversely related to the engine's thermal efficiency [52]. The change in SFC for all fuel samples in response to engine load and CRs is shown in Figure 5. From no load to 40% load, the SFC dropped significantly, and then fell progressively as the load increased. This was due to increased engine power at higher loads, with a lower proportion of heat losses [51]. Diesel had the lowest SFC of all the fuel samples, owing to its greater calorific value and lower density [55]. As the calorific value of biodiesel is low, the SFC of the blends increased with the increase in its blend ratio. Figure 5 shows that increasing the CR reduced the SFC of the fuel samples.

This is because a greater CR encourages the establishment of a better air/fuel ratio, and a higher in-cylinder temperature may aid complete combustion, resulting in lower fuel use [56]. CR 18:1 resulted in the lowest SFC of 0.28 kg/kWh, 0.295 kg/kW-h, 0.3 kg/kWh, 0.31 kg/kWh, 0.33 kg/kWh for diesel, SME10, SME20, SME30 and SME40, respectively.

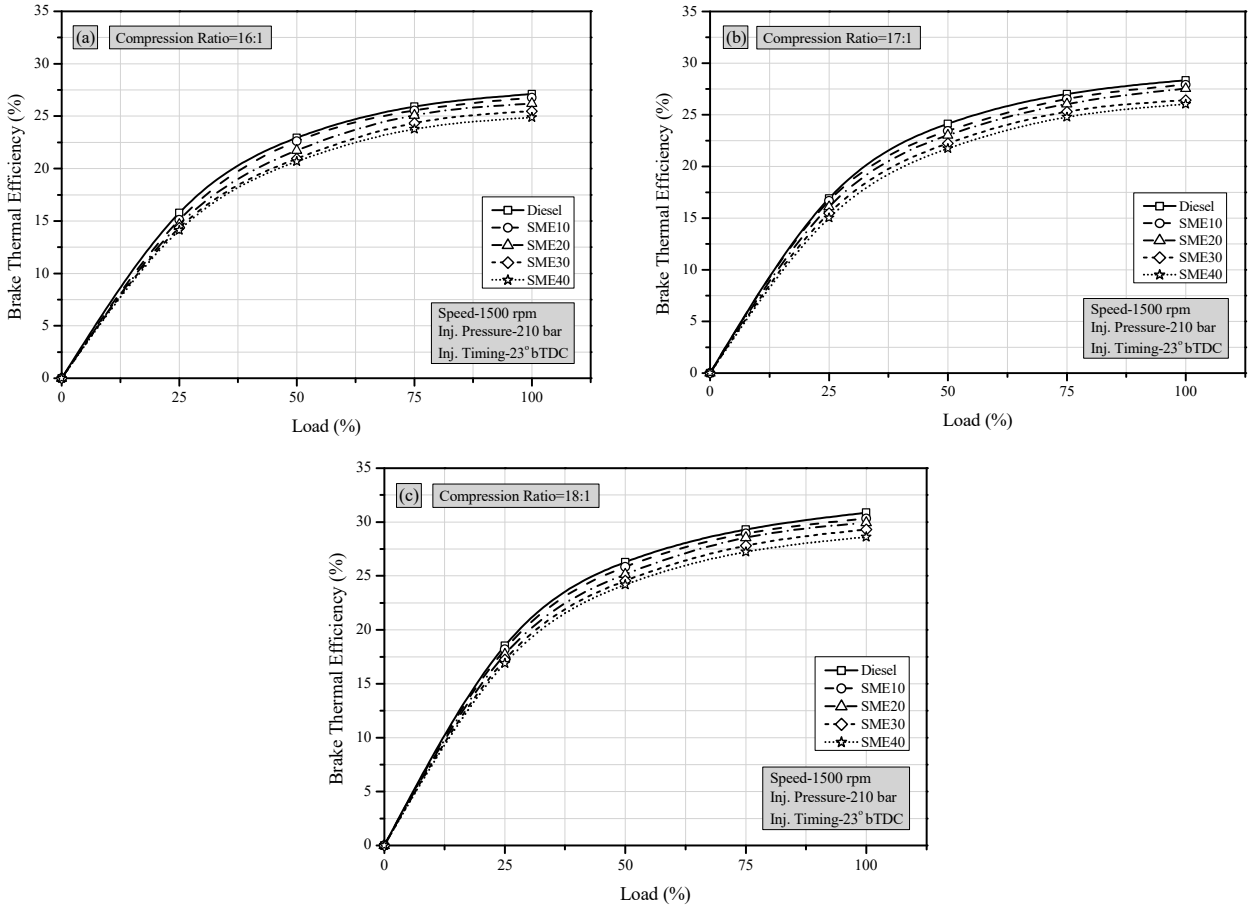

Figure 4. Variation of BTHE with load for the fuel blends at CRs: (**a**) 16:1 (**b**) 17:1 (**c**) 18:1.

Exhaust gas temperature (EGT) indicates the quantity of heat released in the final phases of combustion [57]. Numerous variables influence the EGT of a diesel engine, including the heat release rate, combustion duration, and impact of afterburning, and also the engine operating parameters, including CR and injection pressure [47]. The higher the EGT, the greater will be the heat loss from the engine and, as a result, the lower the BTHE. The variance in EGT for all fuel samples in response to engine load and CRs is shown in Figure 6. From the figure, it can be seen that, as the engine's load increased, the EGT also rose, owing to the increasing fuel quantity in the engine [57]. In comparison to diesel, the blends had higher EGT values. This may have been attributable to the delayed burning of high viscosity blends, and the effects of unburned fuel, which raised EGT in the pre-mixed combustion phase. Additionally, the increased heat loss of the blends also contributed to higher EGT [47]. From Figure 6, it can be seen that the EGT dropped as the CR increased. This may have been due to the compressed air entering the suction stroke at a higher CR, which raised the air temperature. The higher the air temperature, the more the fuel atomizer, resulting in complete combustion and decreased EGT. At lower CRs, the EGT for all the fuel samples was noted to be higher because more heat is generated during the diffusion phase, resulting in a greater amount of heat being carried along with the exhaust gas [22]. CR 18:1 provided the lowest EGT of 314 °C, 329 °C, 338 °C, 352 °C, and 363 °C for diesel, SME10, SME20, SME30 and SME40, respectively.

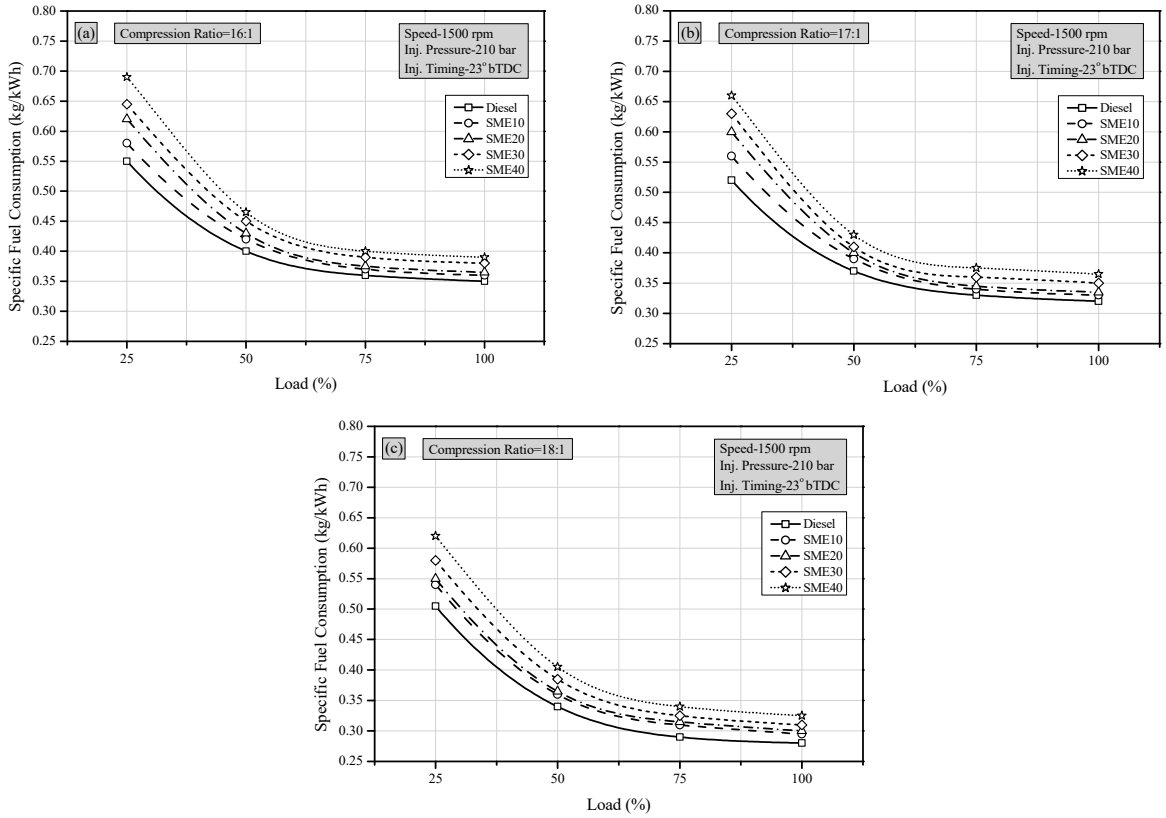

Figure 5. Variation of SFC with load for the fuel blends at CRs: (**a**) 16:1 (**b**) 17:1 (**c**) 18:1.

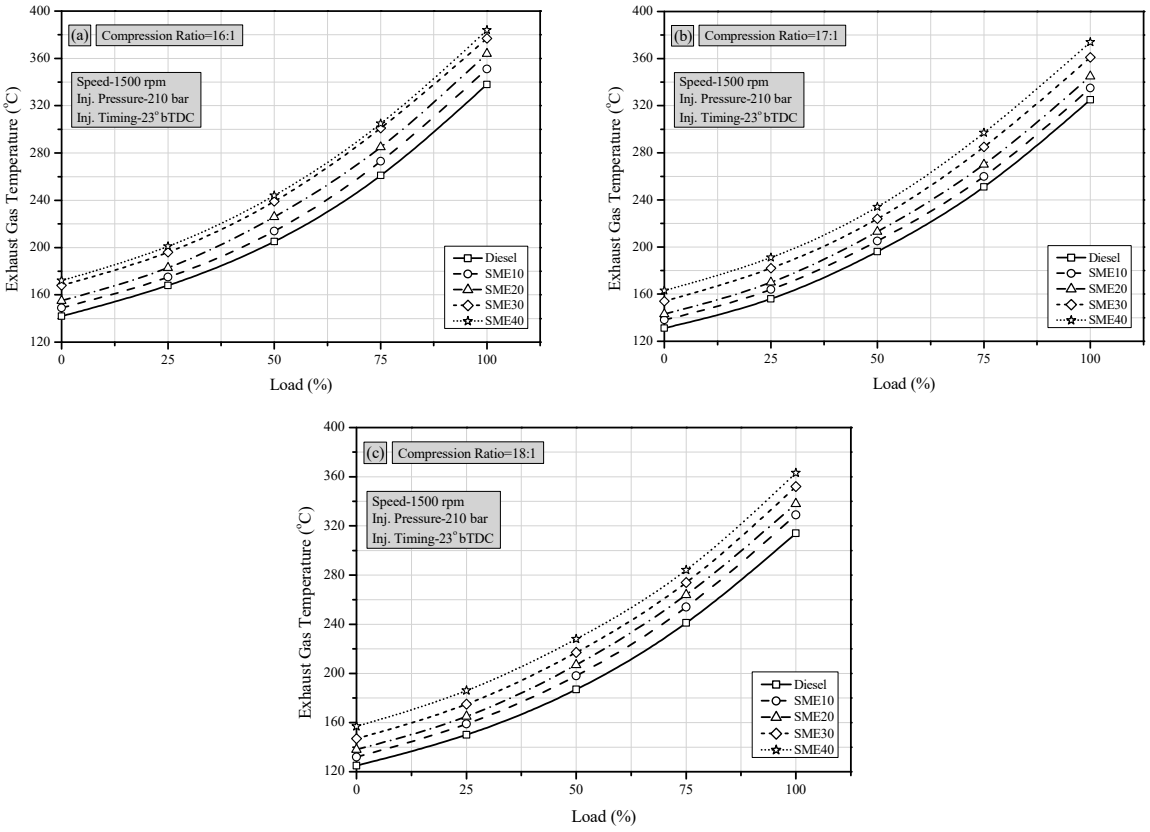

Figure 6. Variation of EGT with load for the fuel blends at CRs: (**a**) 16:1 (**b**) 17:1 (**c**) 18:1.

3.3. Emission Analysis

Carbon monoxide (CO) emissions are primarily produced as a result of incomplete combustion. Incomplete combustion occurs when there is insufficient oxygen for complete burning. Fuel composition, air/fuel ratio, CR, injection pressure and spray penetration all have an impact on incomplete combustion [58]. Figure 7 depicts the variance in CO emissions with engine load for all fuel samples at different CRs. The CO emissions of the fuel samples dropped until they reached 60% load, then rose until they reached the maximum load. The engine's gas temperature remained low under low loads, resulting in incomplete gas-phase combustion and significant CO emissions. The CO oxidation rate increased as the temperature of the gas inside the cylinder climbed to 60% load, resulting in lower CO emissions. When the engine was fully loaded, the amount of fuel injected was high, and the fuel distribution became unequal. As a result, there was inadequate mixing, leading to high CO concentration [54]. At varying engine loads, all of the fuel blends provided lower CO emissions than diesel fuel. This was due to biodiesel fuels having a greater oxygen concentration than diesel fuel, which improved the oxidation process, resulting in reduced CO emissions [57]. CO emission reduced with the increase in CR, as seen in Figure 7. Increasing the CR could result in a shorter delay time, resulting in better and more complete fuel combustion, and hence reduced CO emissions [22]. It was observed that CR 18:1 produced the lowest CO emissions of the test fuels, with 0.24%, 0.22%, 0.205%, 0.195% and 0.19% for diesel, SME10, SME20, SME30 and SME40, respectively.

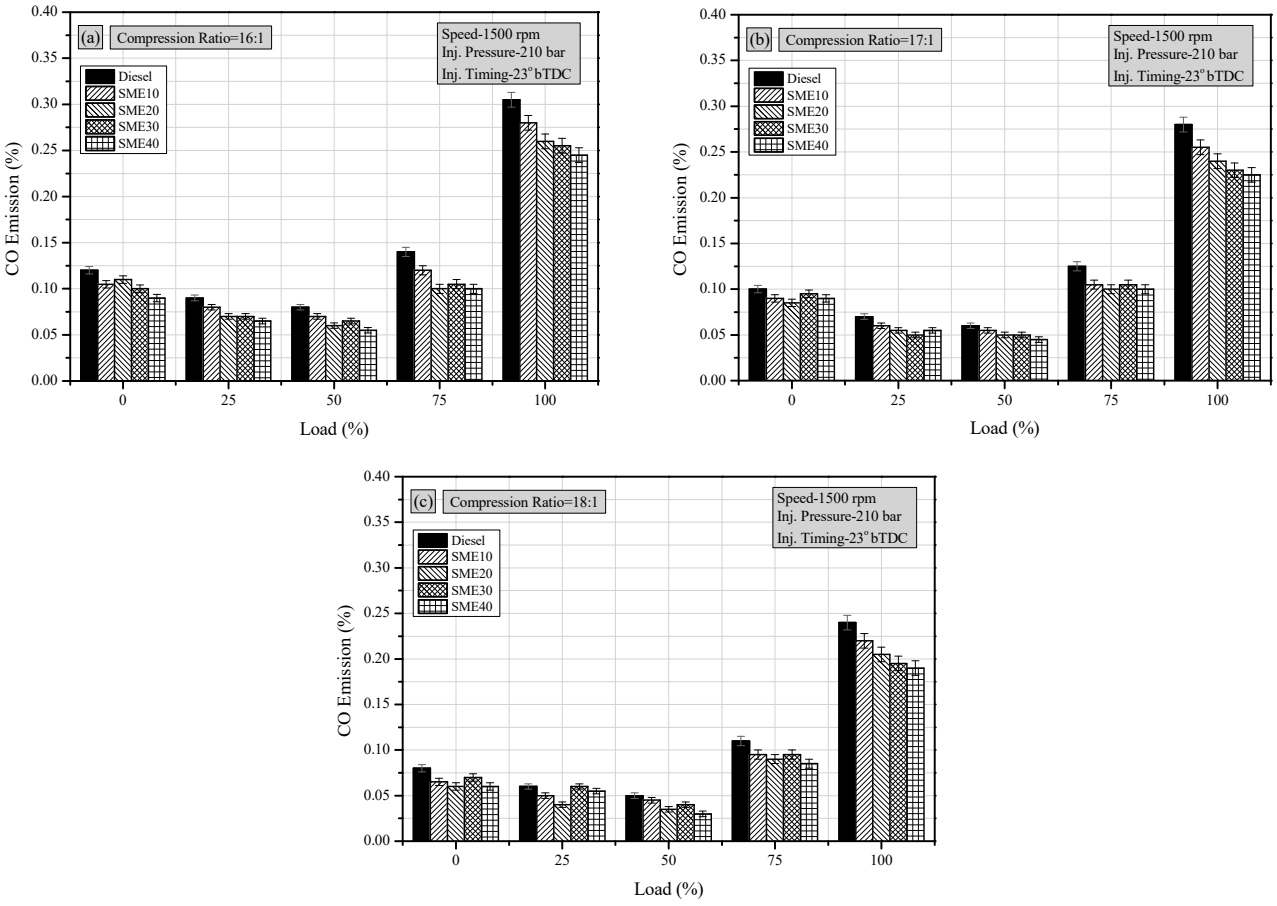

Figure 7. Variation of CO with load for the fuel blends at CRs: (**a**) 16:1 (**b**) 17:1 (**c**) 18:1.

The formation of hydrocarbon (HC) emissions is caused by the same factors that cause CO emissions, which is incomplete combustion [57]. Incomplete fuel–air mixing, quenching of the oxidation process, and a greater carbon-to-oxygen ratio are also major causes of HC emissions [43]. Figure 8 demonstrates the fluctuation in CO emission with engine load

for all the fuel samples at different CRs. According to the graphs, the HC emissions rose with increasing load for all fuels, which was due to the existence of fuel-rich mixes and insufficient oxygen for combustion at higher loads. In addition, when more fuel was fed to the engine, the engine was more likely to undergo incomplete combustion. Such conditions develop when engine loads increase, causing an increase in HC emissions [57]. All the blended fuels were noted to have provided lower HC emissions than pure diesel. This was due to the beneficial impact of high oxygen levels in the combustion chamber, which sped up the oxidation of produced soot at high temperatures [59]. Figure 8 shows that the HC emissions decreased with the increase in CR. This was because higher CRs provide higher in-cylinder temperature and pressure, which enhances fuel combustion and results in reduced HC emissions [60]. For diesel, SME10, SME20, SME30, and SME40, the lowest HC emissions were achieved at CR 18:1, with 53%, 47 %, 45%, 42% and 41%, respectively.

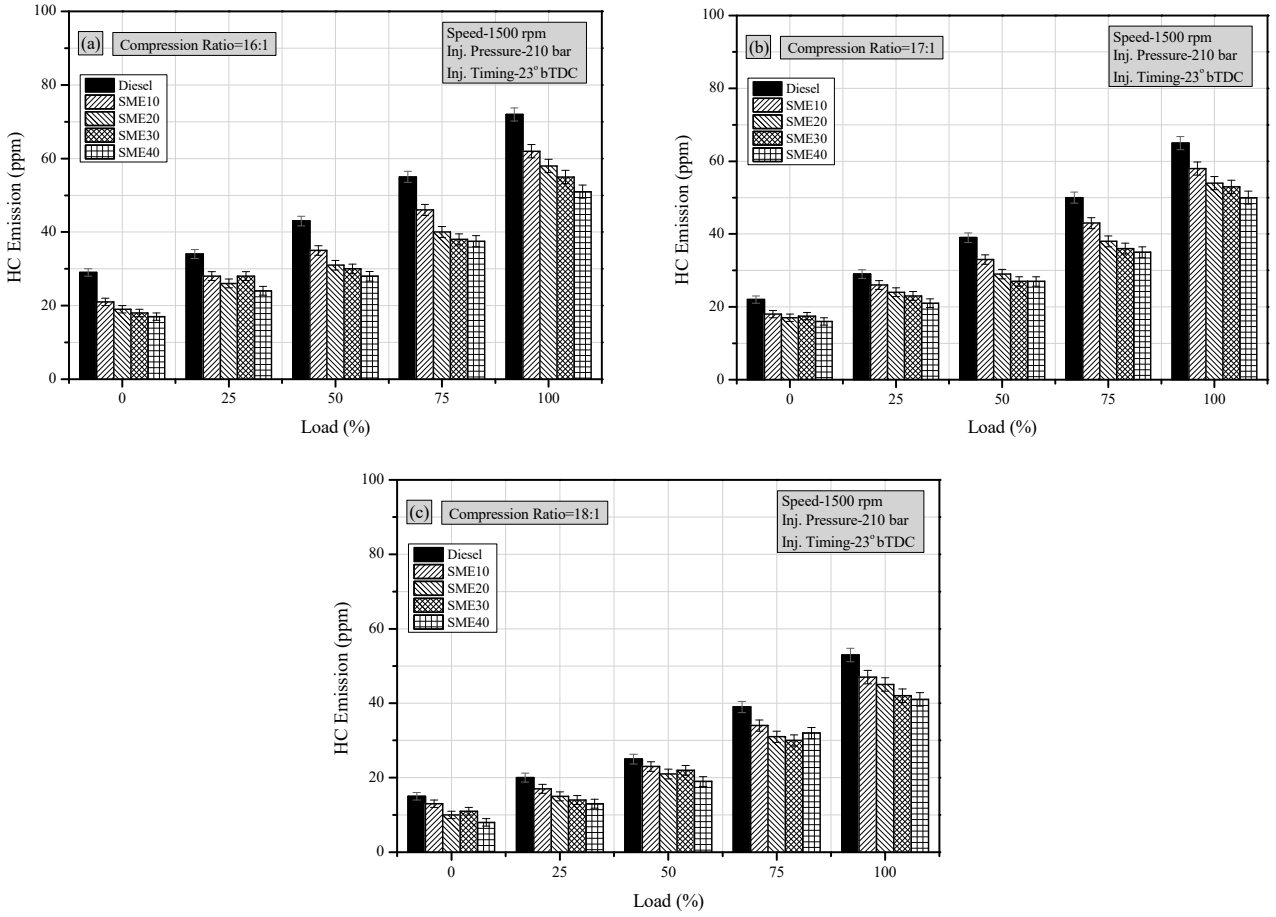

Figure 8. Variation of HC with load for the fuel blends at CRs: (**a**) 16:1 (**b**) 17:1 (**c**) 18:1.

Nitrogen oxides (NO_x) are primarily composed of NO, with minor quantities of NO_2. Other nitrogen oxides, such as N_2O_5, NO_3, and N_2O, are minimal under most situations. The thermal NO_x process—which is influenced by the burned mixture's local temperature, the air/fuel ratio, and the cylinder's residence time at high temperatures—dominates NO_x creation in diesel engines. The reactions involved in this process were initially defined by Zeldovich, and then subsequently expanded to the modified Zeldovich mechanism, which is represented by Equations (4)–(6):

$$N_2 + O \leftrightarrow NO + N \quad (4)$$

$$N + O_2 \leftrightarrow NO + O \quad (5)$$

$$N + OH \leftrightarrow NO + H \quad (6)$$

Figure 9 shows the variation in NO_x emission with engine load for all fuel samples at different CRs. According to the findings, NO_x emissions rose in direct proportion to the fuel load. Lower in-cylinder temperatures at reduced loads resulted from lean fuel–air mixing and less fuel usage, leading to lower NO_x emissions. The rise in the flame temperature, as well as the in-cylinder temperature, as the engine ramped up to full load, increased the generation of thermal NO_x, as a result of more fuel addition at higher load conditions. NO_x emissions were caused not just by high temperatures and pressures, but also by the chemical qualities of the fuel. High fuel density may also have resulted in increased NO_x emissions, as more fuel was retained in the combustion chamber, leading to higher regional temperature values [61]. Biodiesel was observed to have greater NO_x values than diesel, because of its higher oxygen content and density. Due to the blend's higher oxygen content, more nitrogen atoms reacted with it, increasing the NO_x emissions [10]. Higher CRs increased NO_x emissions. This was because of the greater temperature within the cylinder, and the natural oxygen content in biodiesel, which caused pollutants like nitric acid and nitrogen dioxide to develop. [52]. Furthermore, improved combustion may have been responsible for higher NO_x, as it led to a higher temperature during combustion [62]. The least NO_x emissions were obtained at CR 16:1, and were noted to be 971 ppm, 1012 ppm, 1052 ppm, 1086 ppm, and 1132 ppm for diesel, SME10, SME20, SME30 and SME40 respectively. However, the NO_x emissions increased at CR 18:1, and the values were recorded to be 1116 ppm, 1171 ppm, 1193 ppm, 1225 ppm, and 1277 ppm for diesel, SME10, SME20, SME30, and SME40, respectively.

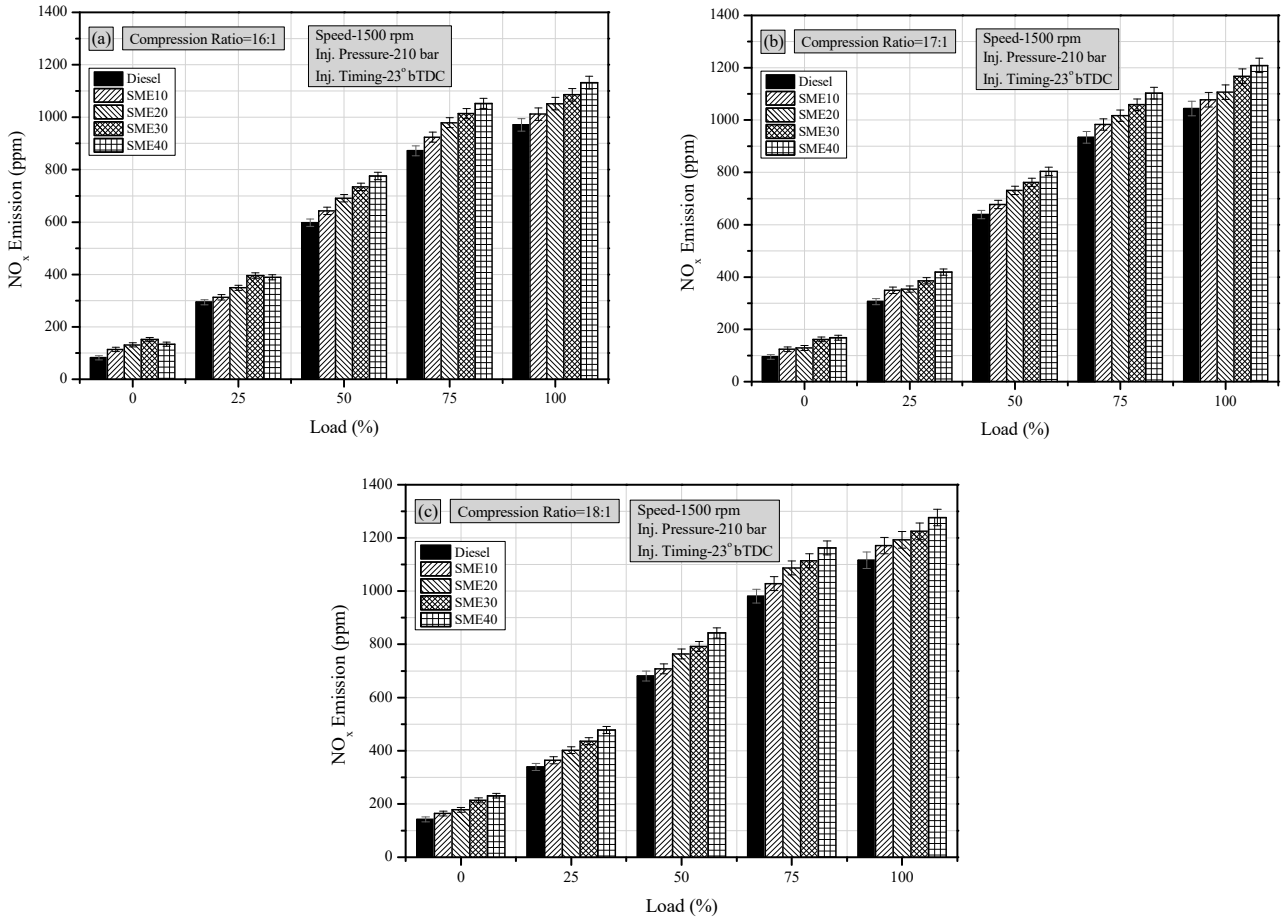

Figure 9. Variation of NO_x with load for the fuel blends at CRs: (**a**) 16:1 (**b**) 17:1 (**c**) 18:1.

Smoke emissions make up the majority of the solid particles released by IC engines. They are the unburned carbon particles that are produced primarily by diesel engines. As the H2 molecules in the liquid fuel droplets in the cylinder react quickly with O_2, and the

residual carbon cannot be burnt because there is not enough O_2, smoke is produced [9]. This may also be described as a qualitative indication of the quantity of bigger diameter particles, which are large enough to disperse the incoming light falling onto the exhaust stream [63]. Figure 10 depicts the variance in smoke emission with engine load for all fuel samples at the various CRs. The smoke levels increased with load for all the fuel samples. The greater number of fuel molecules engaging in oxidation processes at higher loads may have been responsible for this. However, due to a lack of oxygen, at full load, complete combustion did not take place [64]. Furthermore, due to the high temperature and pressure that developed due to the lack of oxygen, smoke was produced in the fuel-rich zone of the cylinder [55]. The use of biodiesel fuel blends resulted in considerable reductions in smoke emissions. This was due to the oxygen content present in the blends of biodiesel, which led to a better oxidation process and improved combustion. In comparison to diesel, which is a non-oxygenated fuel, the presence of oxygen in blends provides more efficient burning in the fuel-rich zones of the combustion chamber, resulting in lowered smoke emissions [63]. With higher CRs, smoke opacity decreased, as seen in Figure 10, which may have been attributable to better fuel–air mixing, which enhanced the combustion process [62]. Moreover, due to the improved fuel atomization, the combustion temperature also rose at higher CRs, leading to reduced smoke values [22]. At CR 18:1, the smoke emissions for diesel, SME10, SME20, SME30, and SME40 were 58.4%, 53.2%, 51.6%, 47.7%, and 48.5%, respectively.

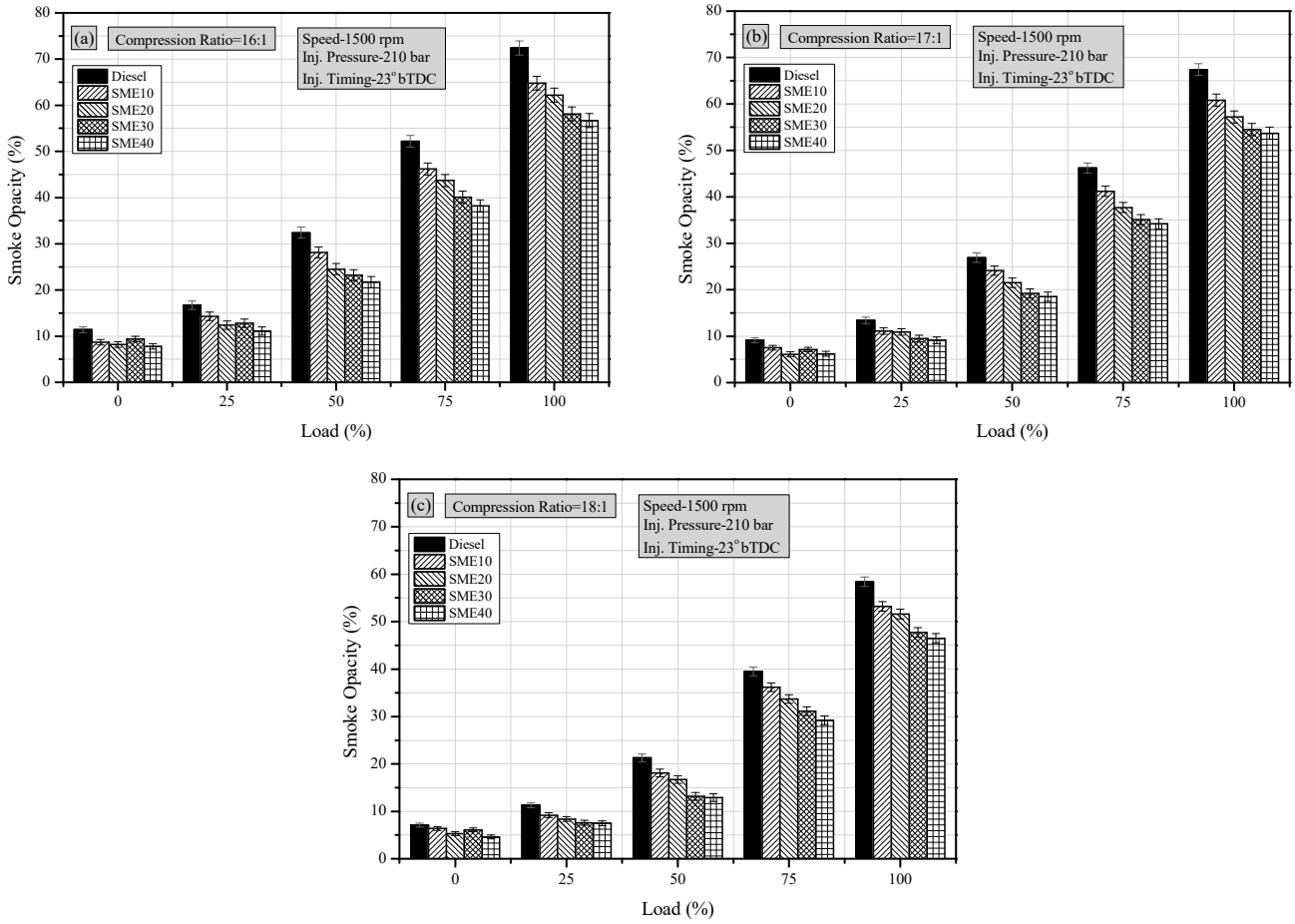

Figure 10. Variation of smoke opacity with load for the fuel blends at CRs: (**a**) 16:1 (**b**) 17:1 (**c**) 18:1.

Factors such as oxygen content, combustion temperature, and reaction residence time are crucial in the production of NO_x emissions. Incomplete combustion brought on by low cylinder temperature and low oxygen concentration, which slow the local oxidation reactions, also contributes to the creation of the CO emission. Additionally, the main

causes of HC emissions include the following: firstly, due to valve overlap during the gas exchange, the unburned mixture in the cylinder escapes into the exhaust port; secondly, as the exhaust valves open, the unburned mixture is forced into the combustion chamber's cracks and discharged, creating the HC emissions; thirdly, during the expansion stroke, particularly during cold starts, the unburned mixture is discharged from the lubricating oil that is utilized to lubricate the piston and piston rings. The combustion chamber's crevices are primarily responsible for the generation of HC emissions [65].

4. Conclusions

Tests were conducted to evaluate the characteristics of a VCR engine run with the blends of sea mango biodiesel/diesel at CRs 16:1, 17:1, and 18:1. This study involved two stages. The first stage included the preparation of biodiesel and the testing of its properties. The second stage dealt with the engine tests when fueled with sea mango biodiesel blends at different CRs. The VCR engine at CR 18:1 had better performance, emission, and combustion characteristics, and hence the values of fuels tested at standard CR 17:1 were compared to those of CR 18:1. The experimental study yielded the following results:

- At CR 18:1, the Cp climbed 13.83% and the HRR fell 11.13%. The CR raised the peak Cp. When CR rose, more secondary fuel was burnable. Peak pressure advancement was projected due to the immediate combustion of gaseous fuel in the cylinder at higher pressure. More oxygen and steady fuel flow may also have raised peak in-cylinder pressure at higher CRs. The HRR decreased with the increase in the CR. This was due to the increase in the maximum in-cylinder temperature, boosting the rate of heat transfer during combustion.
- BTHE rose 8.78% with CR 18:1, compared to the standard CR. Higher CRs in diesel engines led to greater air/fuel mixing, higher combustion chamber temperature, and fine fuel droplet production. As the CR rose, SFC fell. SFC was 11.18% below normal CR at 18:1. Greater CRs enabled higher in-cylinder temperatures, better air/fuel ratios, and full combustion, leading to reduced fuel consumption. At CR 18:1, EGT was also lowered by 2.52%, compared to the standard CR. Compressed air entering the suction stroke at a higher CR boosted the air temperature and improved the combustion, leading to reduced EGT.
- CR reduced CO, HC, and smoke emissions. CR 18:1 decreased CO, HC, and smoke emissions by 14.65%, 18.56%, and 11.56. Shorter delay time, better air–fuel mix, and a greater CR may have been responsible. NOx rose with CR. NO_x values were lower at CR 16:1, while they increased by 6.77% on average at CR 18:1. This was mainly due to the higher in-cylinder temperature and better combustion process at CR 18:1.

Current research reveals sea mango biodiesel blends may be a viable alternative to diesel fuel, with a negligible increase in NOx emissions. Water emulsification or exhaust gas recirculation may reduce the blend's NOx emissions. Further studies may analyze the influence of additives added to sea mango biodiesel blends at varying proportions, assessing engine characteristics.

Author Contributions: Conceptualization, R.R.R., A.J.S., R.Č. and M.E.; Data curation, R.R.R.; Formal analysis, R.R.R.; Investigation, R.R.R.; Methodology, R.R.R., A.J.S., R.Č. and M.E.; Supervision, A.J.S. and R.Č.; Visualization, R.R.R. and M.E.; Writing—original draft, R.R.R. and A.J.S.; Writing—review & editing, R.Č. and M.E. All authors have read and agreed to the published version of the manuscript.

Funding: This research received no external funding.

Institutional Review Board Statement: Not applicable.

Informed Consent Statement: Not applicable.

Data Availability Statement: The data presented in this study are available through email upon request to the corresponding author.

Conflicts of Interest: The authors declare no conflict of interest.

References

1. Kumar, V.; Kalita, K.; Madhu, S.; Ragavendran, U.; Gao, X.Z. A Hybrid Genetic Programming–Gray Wolf Optimizer Approach for Process Optimization of Biodiesel Production. *Processes* **2021**, *9*, 442. [CrossRef]
2. Abed, K.A.; El Morsi, A.K.; Sayed, M.M.; Shaib, A.A.E.; Gad, M.S. Effect of waste cooking-oil biodiesel on performance and exhaust emissions of a diesel engine. *Egypt. J. Pet.* **2018**, *27*, 985–989. [CrossRef]
3. Nantha Gopal, K.; Pal, A.; Sharma, S.; Samanchi, C.; Sathyanarayanan, K.; Elango, T. Investigation of emissions and combustion characteristics of a CI engine fueled with waste cooking oil methyl ester and diesel blends. *Alex. Eng. J.* **2014**, *53*, 281–287. [CrossRef]
4. Gupta, K.K.; Kalita, K.; Ghadai, R.K.; Ramachandran, M.; Gao, X.Z. Machine Learning-Based Predictive Modelling of Biodiesel Production—A Comparative Perspective. *Energies* **2021**, *14*, 1122. [CrossRef]
5. da Silva Trindade, W.R.; dos Santos, R.G. Review on the characteristics of butanol, its production and use as fuel in internal combustion engines. *Renew. Sustain. Energy Rev.* **2017**, *69*, 642–651. [CrossRef]
6. Bae, C.; Kim, J. Alternative fuels for internal combustion engines. *Proc. Combust. Inst.* **2017**, *36*, 3389–3413. [CrossRef]
7. Rezania, S.; Oryani, B.; Park, J.; Hashemi, B.; Yadav, K.K.; Kwon, E.E.; Hur, J.; Cho, J. Review on transesterification of non-edible sources for biodiesel production with a focus on economic aspects, fuel properties and by-product applications. *Energy Convers. Manag.* **2019**, *201*, 112155. [CrossRef]
8. Abdul Hakim Shaah, M.; Hossain, M.S.; Salem Allafi, F.A.; Alsaedi, A.; Ismail, N.; Ab Kadir, M.O.; Ahmad, M.I. A review on non-edible oil as a potential feedstock for biodiesel: Physicochemical properties and production technologies. *RSC Adv.* **2021**, *11*, 25018–25037. [CrossRef]
9. Simsek, S.; Uslu, S. Comparative evaluation of the influence of waste vegetable oil and waste animal oil-based biodiesel on diesel engine performance and emissions. *Fuel* **2020**, *280*, 118613. [CrossRef]
10. Simsek, S. Effects of biodiesel obtained from Canola, sefflower oils and waste oils on the engine performance and exhaust emissions. *Fuel* **2020**, *265*, 117026. [CrossRef]
11. Sai, S.B.; Subramaniapillai, N.; Khadhar Mohamed, M.S.B.; Narayanan, A. Effect of rubber seed oil biodiesel on engine performance and emission analysis. *Fuel* **2021**, *296*, 120708. [CrossRef]
12. Uyumaz, A.; Aydoğan, B.; Yılmaz, E.; Solmaz, H.; Aksoy, F.; Mutlu, İ.; İpci, D.; Calam, A. Experimental investigation on the combustion, performance and exhaust emission characteristics of poppy oil biodiesel-diesel dual fuel combustion in a CI engine. *Fuel* **2020**, *280*, 118588. [CrossRef]
13. Mubarak, M.; Shaija, A.; Suchithra, T.V. Experimental evaluation of Salvinia molesta oil biodiesel/diesel blends fuel on combustion, performance and emission analysis of diesel engine. *Fuel* **2021**, *287*, 119526. [CrossRef]
14. Ahamad Shaik, A.; Rami Reddy, S.; Dhana Raju, V.; Govindarajan, M. Combined influence of compression ratio and EGR on diverse characteristics of a research diesel engine fueled with waste mango seed biodiesel blend. *Energy Sources Part A Recover. Util. Environ. Eff.* **2020**, 1–24. [CrossRef]
15. Sivaramakrishnan, K. Investigation on performance and emission characteristics of a variable compression multi fuel engine fuelled with Karanja biodiesel–diesel blend. *Egypt. J. Pet.* **2018**, *27*, 177–186. [CrossRef]
16. Suresh, M.; Jawahar, C.P.; Renish, R.R.; Malmquist, A. Performance evaluation and emission characteristics of variable compression ratio diesel engine using Argemone Mexicana biodiesel. *Energy Sources Part A Recover. Util. Environ. Eff.* **2021**, *43*, 1511–1523. [CrossRef]
17. Dugala, N.S.; Goindi, G.S.; Sharma, A. Experimental investigations on the performance and emissions characteristics of dual biodiesel blends on a varying compression ratio diesel engine. *SN Appl. Sci.* **2021**, *3*, 622. [CrossRef]
18. Vasudeva, M.; Sharma, S.; Mohapatra, S.K.; Kundu, K. Performance and exhaust emission characteristics of variable compression ratio diesel engine fuelled with esters of crude rice bran oil. *Springerplus* **2016**, *5*, 293. [CrossRef]
19. Rosha, P.; Mohapatra, S.K.; Mahla, S.K.; Cho, H.M.; Chauhan, B.S.; Dhir, A. Effect of compression ratio on combustion, performance, and emission characteristics of compression ignition engine fueled with palm (B20)biodiesel blend. *Energy* **2019**, *178*, 676–684. [CrossRef]
20. Bora, B.J.; Saha, U.K. Experimental evaluation of a rice bran biodiesel-biogas run dual fuel diesel engine at varying compression ratios. *Renew. Energy* **2016**, *87*, 782–790. [CrossRef]
21. Datta, A.; Mandal, B.K. An experimental investigation on the performance, combustion and emission characteristics of a variable compression ratio diesel engine using diesel and palm stearin methyl ester. *Clean Technol. Environ. Policy* **2017**, *19*, 1297–1312. [CrossRef]
22. Sharma, A.; Murugan, S. Potential for using a tyre pyrolysis oil-biodiesel blend in a diesel engine at different compression ratios. *Energy Convers. Manag.* **2015**, *93*, 289–297. [CrossRef]
23. El-Kassaby, M.; Nemit-Allah, M.A. Studying the effect of compression ratio on an engine fueled with waste oil produced biodiesel/diesel fuel. *Alex. Eng. J.* **2013**, *52*, 1–11. [CrossRef]
24. Muralidharan, K.; Vasudevan, D. Performance, emission and combustion characteristics of a variable compression ratio engine using methyl esters of waste cooking oil and diesel blends. *Appl. Energy* **2011**, *88*, 3959–3968. [CrossRef]
25. Suresh, M.; Jawahar, C.P.; Richard, A. A review on biodiesel production, combustion, performance, and emission characteristics of non-edible oils in variable compression ratio diesel engine using biodiesel and its blends. *Renew. Sustain. Energy Rev.* **2018**, *92*, 38–49. [CrossRef]

26. Duan, X.; Lai, M.C.; Jansons, M.; Guo, G.; Liu, J. A review of controlling strategies of the ignition timing and combustion phase in homogeneous charge compression ignition (HCCI) engine. *Fuel* **2021**, *285*, 119142. [CrossRef]
27. Duan, X.; Liu, Y.; Liu, J.; Lai, M.C.; Jansons, M.; Guo, G.; Zhang, S.; Tang, Q. Experimental and numerical investigation of the effects of low-pressure, high-pressure and internal EGR configurations on the performance, combustion and emission characteristics in a hydrogen-enriched heavy-duty lean-burn natural gas SI engine. *Energy Convers. Manag.* **2019**, *195*, 1319–1333. [CrossRef]
28. Pawar, S.K.P.D.A.A. Performance Evaluation and Emission Testing of Sea Mango Seeds Oil Biodiesel Blends in CI Engine. *Int. J. Sci. Res.* **2017**, *6*, 725–729.
29. Kansedo, J.; Lee, K.T.; Bhatia, S. Cerbera odollam (sea mango) oil as a promising non-edible feedstock for biodiesel production. *Fuel* **2009**, *88*, 1148–1150. [CrossRef]
30. Lie, J.; Rizkiana, M.B.; Soetaredjo, F.E.; Ju, Y.H.; Ismadji, S. Production of biodiesel from sea mango (*Cerbera odollam*) seed using in situ subcritical methanol–water under a non-catalytic process. *Int. J. Ind. Chem.* **2018**, *9*, 53–59. [CrossRef]
31. Gaillard, Y.; Krishnamoorthy, A.; Bevalot, F. Cerbera odollam: A "suicide tree" and cause of death in the state of Kerala, India. *J. Ethnopharmacol.* **2004**, *95*, 123–126. [CrossRef]
32. Ong, H.C.; Silitonga, A.S.; Mahlia, T.M.I.; Masjuki, H.H.; Chong, W.T. Investigation of biodiesel production from cerbera manghas biofuel sources. *Energy Procedia* **2014**, *61*, 436–439. [CrossRef]
33. Ang, G.T.; Ooi, S.N.; Tan, K.T.; Lee, K.T.; Mohamed, A.R. Optimization and kinetic studies of sea mango (Cerbera odollam) oil for biodiesel production via supercritical reaction. *Energy Convers. Manag.* **2015**, *99*, 242–251. [CrossRef]
34. Liu, P.C.; Liu, M.H.; Chen, S.Y.; Cherng, W.J.; Wang, C.H. Sea mango cardiac intoxication. *Acta Cardiol. Sin.* **2008**, *24*, 56–59.
35. Kansedo, J.; Lee, K.T. Esterification of hydrolyzed sea mango (*Cerbera odollam*) oil using various cationic ion exchange resins. *Energy Sci. Eng.* **2014**, *2*, 31–38. [CrossRef]
36. Mulye, S.; Technology, H. Performance Testing of CI Engine Fuelled with Blends of Fish Oil Biodiesel and Sea Mango Oil Biodiesel with Diesel Performance Testing of CI Engine Fuelled with Blends of Fish Oil Biodiesel and Sea Mango Oil Biodiesel with Diesel. *Int. J. Altern. Fuels* **2017**, *2*, 3–8.
37. Kansedo, J.; Lee, K.T. Transesterification of palm oil and crude sea mango (*Cerbera odollam*) oil: The active role of simplified sulfated zirconia catalyst. *Biomass Bioenergy* **2012**, *40*, 96–104. [CrossRef]
38. Rohith Renish, R.; Amala Justus Selvam, M. A critical review on production process, physicochemical properties, performance and emission characteristics of sea mango biodiesel-diesel blends. *Mater. Today Proc.* **2021**, *44*, 2600–2605. [CrossRef]
39. Kiliç, M.; Uzun, B.B.; Pütün, E.; Pütün, A.E. Optimization of biodiesel production from castor oil using factorial design. *Fuel Process. Technol.* **2013**, *111*, 105–110. [CrossRef]
40. Ramadhas, A.S.; Jayaraj, S.; Muraleedharan, C. Biodiesel production from high FFA rubber seed oil. *Fuel* **2005**, *84*, 335–340. [CrossRef]
41. Roschat, W.; Siritanon, T.; Yoosuk, B.; Sudyoadsuk, T.; Promarak, V. Rubber seed oil as potential non-edible feedstock for biodiesel production using heterogeneous catalyst in Thailand. *Renew. Energy* **2017**, *101*, 937–944. [CrossRef]
42. Raju, V.D.; Venu, H.; Subramani, L.; Kishore, P.S.; Prasanna, P.L.; Kumar, D.V. An experimental assessment of prospective oxygenated additives on the diverse characteristics of diesel engine powered with waste tamarind biodiesel. *Energy* **2020**, *203*, 117821. [CrossRef]
43. Balamurugan, T.; Arun, A.; Sathishkumar, G.B. Biodiesel derived from corn oil—A fuel substitute for diesel. *Renew. Sustain. Energy Rev.* **2018**, *94*, 772–778. [CrossRef]
44. Chandra Sekhar, S.; Karuppasamy, K.; Vedaraman, N.; Kabeel, A.E.; Sathyamurthy, R.; Elkelawy, M.; Alm ElDin Bastawissi, H. Biodiesel production process optimization from Pithecellobium dulce seed oil: Performance, combustion, and emission analysis on compression ignition engine fuelled with diesel/biodiesel blends. *Energy Convers. Manag.* **2018**, *161*, 141–154. [CrossRef]
45. Ramalingam, K.; Balasubramanian, D.; Chellakumar, P.J.T.J.S.; Padmanaban, J.; Murugesan, P.; Xuan, T. An assessment on production and engine characterization of a novel environment-friendly fuel. *Fuel* **2020**, *279*, 118558. [CrossRef]
46. Choudhary, K.D.; Nayyar, A.; Dasgupta, M.S. Effect of compression ratio on combustion and emission characteristics of C.I. Engine operated with acetylene in conjunction with diesel fuel. *Fuel* **2018**, *214*, 489–496. [CrossRef]
47. Baweja, S.; Trehan, A.; Kumar, R. Combustion, performance, and emission analysis of a CI engine fueled with mustard oil biodiesel blended in diesel fuel. *Fuel* **2021**, *292*, 120346. [CrossRef]
48. Venu, H.; Madhavan, V. Influence of diethyl ether (DEE) addition in ethanol-biodiesel-diesel (EBD) and methanol-biodiesel-diesel (MBD) blends in a diesel engine. *Fuel* **2017**, *189*, 377–390. [CrossRef]
49. Alagu, K.; Venu, H.; Jayaraman, J.; Raju, V.D.; Subramani, L.; Appavu, P.; Dhanasekar, S. Novel water hyacinth biodiesel as a potential alternative fuel for existing unmodified diesel engine: Performance, combustion and emission characteristics. *Energy* **2019**, *179*, 295–305. [CrossRef]
50. Ibrahim, A.; El-Adawy, M.; El-Kassaby, M.M. The Impact of Changing the Compression Ratio on the Performance of an Engine fueled by Biodiesel Blends. *Energy Technol.* **2013**, *1*, 395–404. [CrossRef]
51. Hariram, V.; Vagesh Shangar, R. Influence of compression ratio on combustion and performance characteristics of direct injection compression ignition engine. *Alex. Eng. J.* **2015**, *54*, 807–814. [CrossRef]

52. Prasada Rao, G.; Sathya Vara Prasad, L. Combined influence of compression ratio and exhaust gas recirculation on the diverse characteristics of the diesel engine fueled with novel palmyra biodiesel blend. *Energy Convers. Manag. X* **2022**, *14*, 100185. [CrossRef]
53. Jaichandar, S.; Annamalai, K. Effects of open combustion chamber geometries on the performance of pongamia biodiesel in a di diesel engine. *Fuel* **2012**, *98*, 272–279. [CrossRef]
54. Das, M.; Sarkar, M.; Datta, A.; Santra, A.K. An experimental study on the combustion, performance and emission characteristics of a diesel engine fuelled with diesel-castor oil biodiesel blends. *Renew. Energy* **2018**, *119*, 174–184. [CrossRef]
55. Saravanan, A.; Murugan, M.; Sreenivasa Reddy, M.; Parida, S. Performance and emission characteristics of variable compression ratio CI engine fueled with dual biodiesel blends of Rapeseed and Mahua. *Fuel* **2020**, *263*, 116751. [CrossRef]
56. Sayin, C.; Gumus, M. Impact of compression ratio and injection parameters on the performance and emissions of a di diesel engine fueled with biodiesel-blended diesel fuel. *Appl. Therm. Eng.* **2011**, *31*, 3182–3188. [CrossRef]
57. Badawy, T.; Mansour, M.S.; Daabo, A.M.; Abdel Aziz, M.M.; Othman, A.A.; Barsoum, F.; Basouni, M.; Hussien, M.; Ghareeb, M.; Hamza, M.; et al. Selection of second-generation crop for biodiesel extraction and testing its impact with nano additives on diesel engine performance and emissions. *Energy* **2021**, *237*, 121605. [CrossRef]
58. Gharehghani, A.; Hosseini, R.; Mirsalim, M.; Yusaf, T.F. A computational study of operating range extension in a natural gas SI engine with the use of hydrogen. *Int. J. Hydrogen Energy* **2015**, *40*, 5966–5975. [CrossRef]
59. Attia, A.M.A.; Nour, M.; Nada, S.A. Study of Egyptian castor biodiesel-diesel fuel properties and diesel engine performance for a wide range of blending ratios and operating conditions for the sake of the optimal blending ratio. *Energy Convers. Manag.* **2018**, *174*, 364–377. [CrossRef]
60. Gugulothu, S.K. Retracted: Experimental investigation of the influence of combustion chambers and compression ratio on the performance and emission characteristics of diesel engine. *Heat Transf.* **2021**, *50*, 1021. [CrossRef]
61. Chen, H.; Xie, B.; Ma, J.; Chen, Y. NOx emission of biodiesel compared to diesel: Higher or lower? *Appl. Therm. Eng.* **2018**, *137*, 584–593. [CrossRef]
62. Hosamani, B.R.; Katti, V.V. Experimental analysis of combustion characteristics of CI DI VCR engine using mixture of two biodiesel blend with diesel. *Eng. Sci. Technol. Int. J.* **2018**, *21*, 769–777. [CrossRef]
63. Dhar, A.; Agarwal, A.K. Performance, emissions and combustion characteristics of Karanja biodiesel in a transportation engine. *Fuel* **2014**, *119*, 70–80. [CrossRef]
64. Uyumaz, A. Combustion, performance and emission characteristics of a DI diesel engine fueled with mustard oil biodiesel fuel blends at different engine loads. *Fuel* **2018**, *212*, 256–267. [CrossRef]
65. Xu, L.; Sun, X.; Ku, C.; Liu, J.; Lai, M.C.; Duan, X. Effects of control strategies for mixture activity and chemical reaction pathway coupled with exhaust gas recirculation on the performance of hydrogen-enriched natural-gas fueled spark ignition engine. *Fuel* **2022**, *322*, 124153. [CrossRef]